

## Article

# Significant Improvement of Strength in Wrought 945A Ni-Based Superalloy by Aging Treatment

Haiding Liu <sup>1,2</sup>, Dongzhe Wang <sup>3,4</sup>, Linping Zhou <sup>1</sup>, Jia She <sup>5,\*</sup> and Wei Wu <sup>2,3</sup>

<sup>1</sup> College of Materials Science and Engineering, Hunan University, Changsha 410082, China; liuhaiding@cmri.cc (H.L.); lpzhou@hnu.edu.cn (L.Z.)

<sup>2</sup> Chongqing Materials Research Institute Co., Ltd. (CMRI), Chongqing 400707, China; ww\_ui@163.com

<sup>3</sup> Chongqing Key Laboratory of Corrosion-Resistant Alloys, Chongqing 400707, China; wwwwdz@sina.com

<sup>4</sup> National Engineering Research Center for Instrument Functional Materials, Chongqing 400707, China

<sup>5</sup> College of Materials Science and Engineering, Chongqing University, Chongqing 400044, China

\* Correspondence: jiashe@cqu.edu.cn

**Abstract:** Ni-based superalloys have attracted much attention due to their good resistance to high-temperature and -pressure environments. Compared with the traditional 718 Ni-based superalloy, 945A Ni-based superalloy with a lower Ni content showed better performance in terms of precipitated hardening and corrosion resistance. In this study, the aging behavior and the evolution of mechanical properties of the wrought 945A Ni-based superalloy were investigated. Microstructures were analyzed by scanning electron microscopy (SEM), bright field transmission electron microscopy (TEM), high-resolution TEM and high-angle annular dark field scanning TEM. Mechanical properties were measured by tensile and compressive tests. The results illustrated that the compressive yield stress was significantly improved by increasing aging time from 229 to 809 MPa. The increase was greater than 220%. This improvement was mainly attributed to the precipitates of the  $\gamma'$  phase and carbides during the aging treatment. The residual dislocations generated by the plastic processes stimulated the formation of these precipitates. The precipitation behavior and the strengthening mechanism are discussed in detail.

**Keywords:** Ni-based superalloy; aging behavior; precipitate; mechanical property



**Citation:** Liu, H.; Wang, D.; Zhou, L.; She, J.; Wu, W. Significant Improvement of Strength in Wrought 945A Ni-Based Superalloy by Aging Treatment. *Crystals* **2021**, *11*, 627. <https://doi.org/10.3390/cryst11060627>

Academic Editors: Hongbin Bei and Cyril Cayron

Received: 12 March 2021

Accepted: 8 May 2021

Published: 31 May 2021

**Publisher's Note:** MDPI stays neutral with regard to jurisdictional claims in published maps and institutional affiliations.



**Copyright:** © 2021 by the authors. Licensee MDPI, Basel, Switzerland. This article is an open access article distributed under the terms and conditions of the Creative Commons Attribution (CC BY) license (<https://creativecommons.org/licenses/by/4.0/>).

## 1. Introduction

Ni-based superalloys are one type of metal alloy for application in harsh conditions, such as high-temperature, high-pressure and corrosive environments [1,2]. Compared with the traditional Inconel 718 superalloy, Incoloy 945A superalloy with a lower Ni content ( $\approx 47$  wt.%) is a precipitated hardening and corrosion-resistant Ni-Fe-Cr alloy, which presents excellent strength, ductility and resistance to corrosion cracking [3].

Similar to the traditional 718 Inconel superalloy, the matrix of 945A superalloy is a face centered cubic (FCC) structure known as gamma ( $\gamma$ ) phase. The main second phases of the 945A superalloy are  $\gamma'$  ( $\text{Ni}_3(\text{Al}, \text{Ti}, \text{Nb})$ ) and  $\gamma''$  ( $\text{Ni}_3\text{Nb}$ ) [4]. The second phases can be obtained by using different heat-treatment processes. According to Hagel [5], the  $\gamma'$  phase is a stable phase and has a low misfit with the  $\gamma$  matrix, which is only 0.1%. Moreover, the  $\gamma'$  phase presents an  $\text{A}_3\text{B}$  type, in which 'A' is the Ni element and 'B' can be replaced by Al, Ti and Nb [6,7]. The  $\gamma''$  phase is reported to be a metastable phase and can only occur below the heat treatment temperature of 650 °C [8,9].

In previous investigations of Ni-base superalloys [10], aging treatment has generally been performed on alloys in the as-cast condition. However, in actual applications, many metal alloys are usually processed using plastic deformation, such as extrusion, forging and rolling [11,12]. Compared with the as-cast metal alloys, metal alloys subjected to plastic processing usually have a fine microstructure and better mechanical properties [13,14]. At present, there are few studies on post-deformation heat treatment of Ni-base superalloys.

Due to plastic deformation, a large number of defects will be generated. In the subsequent heat-treatment process, the alloying elements tend to segregate at the defects [15]. This segregation behavior can stimulate the formation of precipitates and affect the distribution of precipitates [16]. Corresponding phenomena have been widely reported in Mg and Al alloys [17,18]. For Ni-base superalloys, the types of alloying elements are more numerous, and their contents are much higher than those in Mg and Al alloys. For example, the 945A superalloy has high contents of Fe and Cr (>15 wt.%) [19]. For these reasons, element segregation and precipitation are more likely to occur in Ni-based superalloys. However, precipitation at defects and the improvement in mechanical properties in Ni-based superalloys are still unclear.

In this work, the 945A Ni-based superalloy was selected as the object to investigate the aging behavior after plastic deformation. The sample was deformed by forging and rolling processes. The aging behavior and the mechanical property evolution of the wrought 945A Ni-based superalloy were investigated in detail. Study of the aging behavior of the 945A Ni-based alloy can allow for industrial applications under high-temperature conditions, such as in generator sets, supercritical and ultra-supercritical conditions.

## 2. Materials and Methods

The as-cast material was fabricated by the vacuum induction melting plus electroslag remelting duplex smelting process. The main alloying elements were Fe, Cr, Nb, Mo, Cu, Ti, Mn, and Al. The rest was the Ni matrix. After the casting process, an ingot with a diameter of  $\Phi 160$  mm was obtained. The height of the ingot was 100 mm. The chemical compositions of the as-cast 945A Ni-based alloy were detected by an X-ray fluorescence spectrometer (XRF, 800CCDE, Shimadzu Corporation, Shimadzu, Japan). The weight percentages of element contents are listed in Table 1. The ingot was subjected to hot forging and rolling processes, resulting in a bar of 16 mm in diameter. The plastic processes were as follows. First, the forging process was conducted at 1160 °C, and finished at 950 °C. Then, the cross-section of the ingot was forged from 160 mm in diameter to 40 mm  $\times$  40 mm. After the forging process, the rolling process was conducted at 1160 °C, and finished at 950 °C. The cross-section of the sample was deformed from 40 mm  $\times$  40 mm to 16 mm in diameter. The solid solution treatment of the wrought bars was processed at 1060 °C for 1 h. The cooling method was water quenching.

**Table 1.** The chemical composition (in weight percentage, wt.%) of the 945A Ni-based superalloy.

Alloy	Fe	Cr	Nb	Mo	Cu	Ti	Mn	Al	Other	Ni
945ANi-based superalloy	18.3	21.7	4.0	3.6	1.8	1.0	0.5	0.5	0.3	48.3

The aging treatment parameters are listed in Table 2. The aging temperature was 725 °C, and the aging times were 1, 4, 8, 16 and 32 h. The cooling method was air cooling. The five samples of different aging times were designated as i, ii, iii, iv and v, respectively. After the aging treatments, scanning electron microscopy (SEM) and transmission electron microscopy (TEM) were employed to study the second-phase evolution. The samples for SEM observation were polished to a mirror finish by using silicon carbide papers (P240–P2500) and a mechanical polishing machine. The second-phase and grain boundaries were revealed using Kalling's reagent etchant, which is a mixed solution of 100 mL ethanol, 100 mL HCl and 5 g CuCl<sub>2</sub>. The SEM test was conducted on the TESCAN VEGA 3 LMH SEM (TESCAN, Brno-Kohoutovice, Czech Republic). The acceleration voltage for SEM was 10 kV, while the Energy Dispersive Spectroscopy (EDS) was 20 kV. The probe current was 8 pA. The operation distance was 10 mm. The TEM samples were mechanically polished to thin foils with a thickness of less than 100  $\mu$ m. The surface of the polished sample was like a mirror. We then used a precise ion polishing system (PIPS II 695, Gatan, Pleasanton, CA, USA) to reduce the thickness of the sample to less than 100 nm. The TEM test was conducted on the Philips TECNAI 20, Santa Clara, CA, USA. The acceleration voltage was

200 kV. The TEM data were analyzed by the Digital Micrograph software (Version 3, Ganta, Pleasanton, CA, USA).

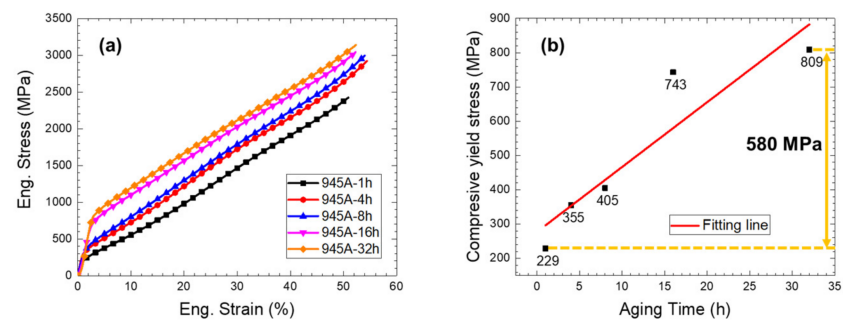
**Table 2.** The parameters of the aging treatment on the 945A Ni-based superalloy.

Sample Number	Temperature (°C)	Aging Time (h)
945A-1h	725	1
945A-4h	725	4
945A-8h	725	8
945A-16h	725	16
945A-32h	725	32

The samples were cut to  $\Phi 3 \text{ mm} \times 6 \text{ mm}$  to evaluate the compressive properties. The compressive test was performed on the CMT6305-300KN electronic universal testing machine (Skyan power equipment Ltd., Shenzhen, China) at room temperature. Every sample was tested three times to guarantee the repetition ratio of the curves. The strain rate of the compressive test was  $1 \times 10^{-3} \text{ s}^{-1}$ .

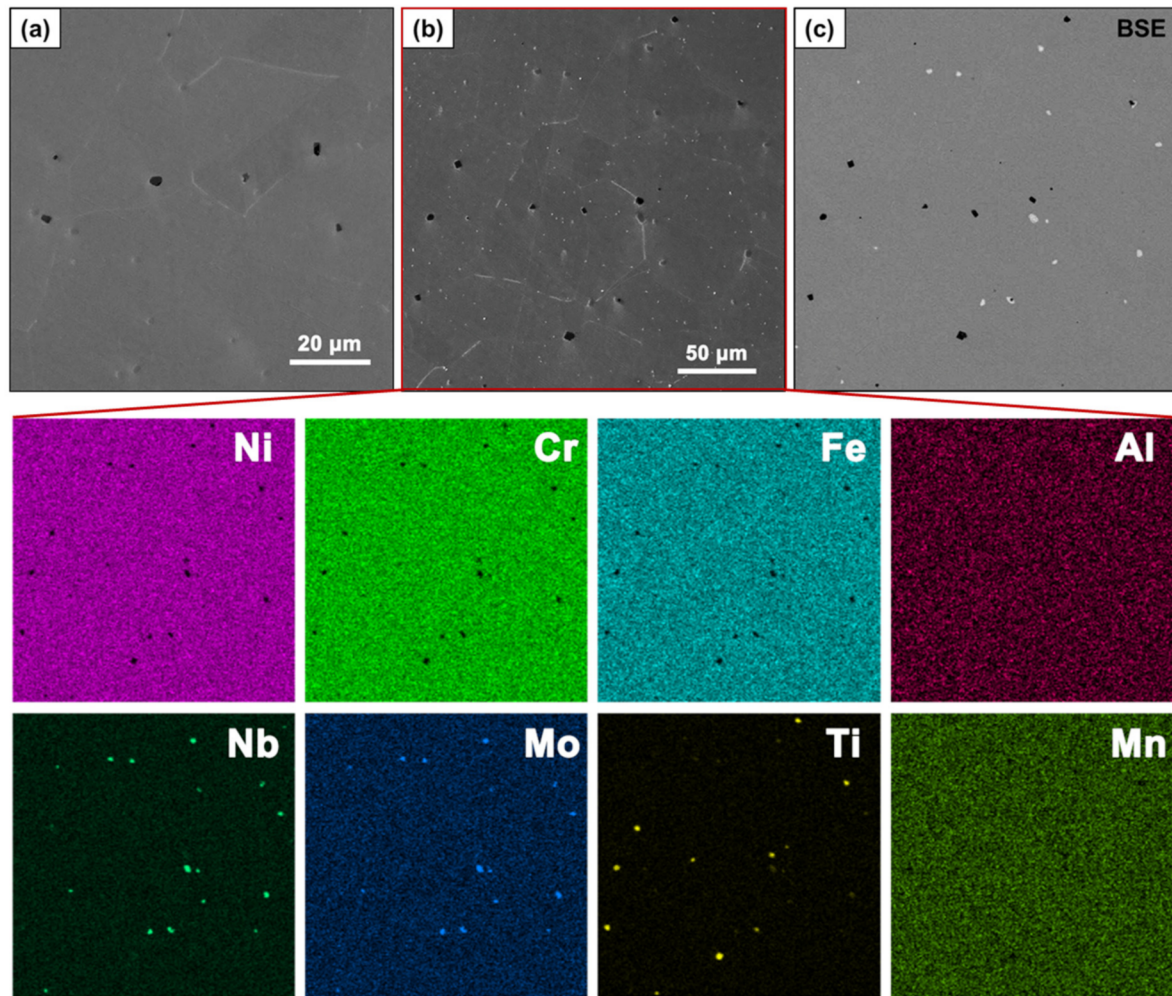
### 3. Results

Figure 1 shows the compressive properties of the five samples with different aging times. The compressive curves in Figure 1a, show that the compressive yield stress was significantly improved by increasing the aging time. The compressive yield stresses of the 945A-1h, 945A-4h, 945A-8h, 945A-16h and 945A-32h samples were 229, 355, 405, 743 and 809 MPa, respectively. The relevant data are displayed in Figure 1b. With the increase in aging time, the compressive yield stress shows a trend of linear increase due to the precipitate behavior during the aging treatment. Compared to the 945A-1h sample, the compressive yield stress of 945A-32h sample increased by 580 MPa. The increase was as much as 220%.



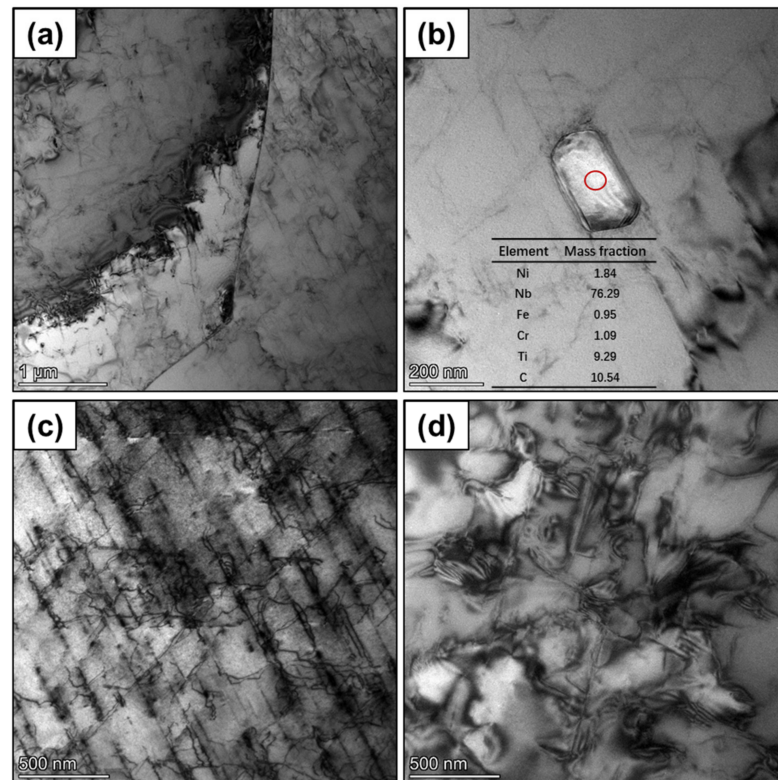
**Figure 1.** The compressive properties of the 945A Ni-based superalloys. (a) Compressive curves, and (b) the compressive yield stress vs. aging time distribution map.

The SEM results of the non-heat-treated and 945A-32h samples are shown in Figure 2. In Figure 2a, some coarse second-phase particles could be found in the non-heat-treated sample. With the increase in aging time, both coarse and fine particles were observed in the 945A-32h samples (Figure 2b). The coarse particles could be divided into two types: one type exhibited a black square shape and the other, a white square shape, as shown in the backscattered electron (BSE) results of Figure 2c. According to the EDS mapping analysis results, the black square shaped particles were enriched with Ti, and the white square shaped particles were enriched with Nb and Mo. These coarse particles were most apparent in the micron scale and were considered to be carbides or nitrides. The coarse particles were thermally stable and still existed after solid solution treatment [20,21]. According to Saleem et al. [19], these black square-shaped particles enriched with Ti were TiN. The white square shaped particles were considered to be carbide. The fine particles, were mainly at the nanoscale and too small to identify with the SEM.



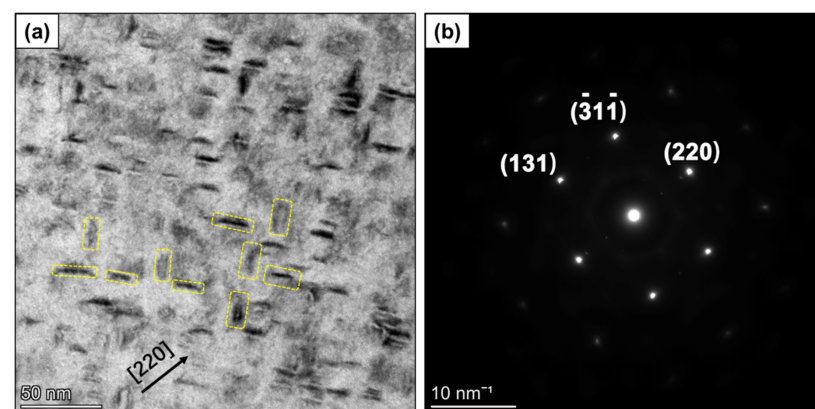
**Figure 2.** The SEM micrograph and the EDS mapping distributions of the aging treatment samples, (a) secondary electron image of the non-heat treated sample, (b) secondary electron image of the 945A-32h sample and (c) BSE image of the 945A-32h sample. The EDS mapping images were detected in the area of Figure 2b.

Figure 3 shows the TEM images of the 945A-32h sample. After the plastic processes, many dislocations were formed in the matrix, as shown in Figure 3a. Meanwhile, particles with a size of ~200 nm could be found on the matrix, as shown in Figure 3b. According to the EDS point analysis results in Figure 3b, the particles were mainly enriched by Nb, Ti and C, which was considered a carbide. Residual dislocations were divided into two types. One was a movable dislocation, which appeared as banding. The other was a dislocation entanglement region, characterized by high strain. These dislocation lines and the high-strain region were beneficial to the formation of the precipitated phase.



**Figure 3.** The bright field TEM images of the 945A-32h sample, (a) the grain boundaries and the dislocations, (b) the second phase morphology, (c,d) magnified images of the dislocations.

Meanwhile, many nanoscale precipitates were observed in Figure 4. The size of the precipitates was 10–20 nm and the space between these precipitates was 5–10 nm. Such a high density of precipitates illustrated that a large fraction of the solid alloy was precipitated. Under the spatial axis of (220), two different direction distributions of the precipitates were found. These two directions were perpendicular to each other as marked by the yellow box. According to the literature [22], precipitates with such a microstructure in 945 Ni-based alloys are considered to be  $\gamma'$  phase. The  $\gamma'$  phase was precipitated on the (110) plane of the matrix. The high density of the  $\gamma'$  phase is beneficial in improving the mechanical properties after aging treatment.



**Figure 4.** The TEM image of the nanoscale precipitations in 945A-32h sample, (a) the bright field TEM image of the precipitates, (b) the selected area diffraction image.

#### 4. Discussion

It can be seen from the results that the aging time of wrought 945A Ni-based superalloy has a great effect on its mechanical properties. The existence of the dislocations in the wrought 945A Ni-based superalloy were conducive to the subsequent precipitation of the  $\gamma'$  phase during the aging treatment. Therefore, the precipitation behavior of the  $\gamma'$  phase and the strengthening mechanism of the second phase in the 945A-32h sample are discussed in the following sections.

##### 4.1. The Precipitation Behavior of the $\gamma'$ Phase

In order to identify the precipitation behavior of the  $\gamma'$  phase, high-angle annular dark field scanning transmission electron microscopy (HAADF-STEM) was employed to analyze the microstructure and the element composition of the  $\gamma'$  phase. Figure 5 shows the HAADF-STEM image and the EDS mapping distribution of  $\gamma'$  phase in the 945A-32h sample. In the HAADF-STEM image, the  $\gamma'$  phase particles present as the white square shapes, and the matrix as the dark background. According to the EDS mapping distributions, these white square particles are enriched with Ni, Ti and Nb. The distributions of these precipitates were parallel to each other, which was consistent with the results in Figure 4. A similar distribution was found in an investigation of ATI 718Plus [23], which was aged at a different temperature (675 °C for 8 h and 788 °C for 4 h).

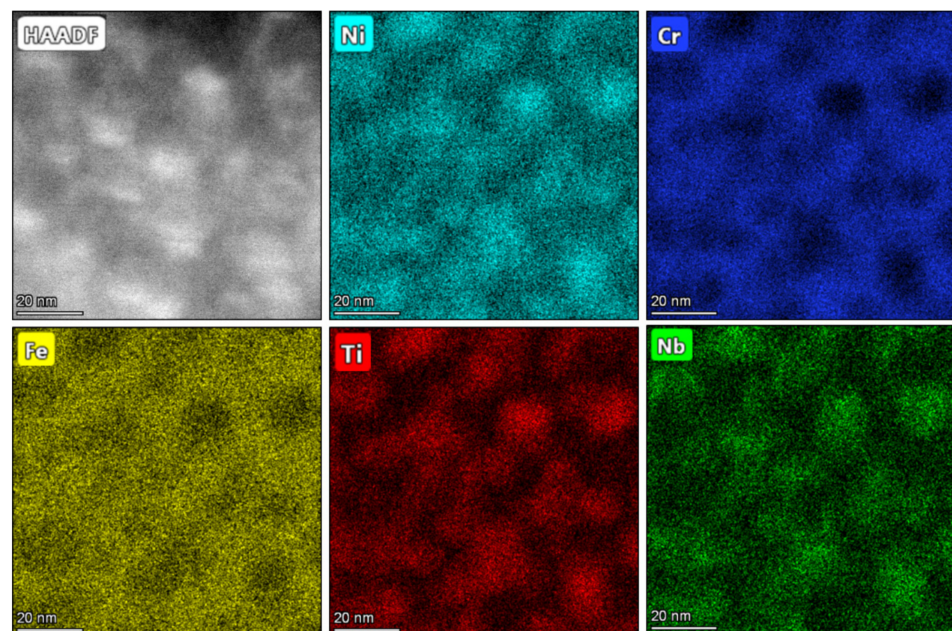


**Figure 5.** The HAADF-STEM image and the EDS mapping distribution of  $\gamma'$  phase in the 945A-32h sample.

It is accepted that the precipitation of the 945 Ni-based superalloy contains  $\gamma'$ ,  $\gamma''$ ,  $M_{23}C_6$ ,  $\eta$  and  $\delta$  phases [19,24]. According to the TTT curve investigation of Mannan [25], the  $\eta$  and  $\delta$  phase in the 945 Ni-based superalloy only occurs at temperatures higher than 750 °C and that with aging at 600–750 °C, the precipitations are  $\gamma'$ ,  $\gamma''$  and  $M_{23}C_6$  phases. In this study, the aging temperature was 725 °C, which means the main precipitates were  $\gamma'$ ,  $\gamma''$  and  $M_{23}C_6$  phases rather than  $\eta$  and  $\delta$  phases. However, in the TEM results of Figures 3 and 4, only  $\gamma'$  was found, i.e., no  $\gamma''$  phase was detected. According to Chaturvedi and Oblak [8,9], the  $\gamma''$  phase is formed from the  $\gamma'$  phase at aging temperatures below 650 °C. Thus, under the aging temperature of 725 °C, the  $\gamma''$  phase was not likely to form. Therefore, besides the carbide, the precipitate in the aging treatment 945A Ni-based superalloy was  $\gamma'$ .

Moreover, the sample in this study was in the wrought condition, which contained many dislocations and deformed regions in the microstructure. During the aging treatment, dislocations and the high strain region are beneficial to stimulate the formation of precipitates. A similar element segregation behavior at defects has been reported in Al and Mg alloys [26,27]. High-resolution TEM analysis was employed to clarify the interaction between the dislocations and the element segregation in the 945A-32h sample. The relevant high-resolution TEM image and the inverse Fourier transform (FFT) image are displayed in Figure 6. There were many dislocations in the element segregation region. The existence of edge-type dislocations (marked with “T” symbols) can be clearly seen in Figure 6b. This suggests that element segregation was more likely to occur near dislocations. In the subsequent heat-treatment process, these elements were precipitated in the segregation region, resulting in fine and dispersed precipitates. Since the dislocation distribution was striped and crossed, these precipitates also tended to be perpendicular to each other after precipitation. This was why the precipitates in Figure 4 were perpendicular to each other. The distribution of the precipitates was conducive to hindering the dislocation movement in subsequent plastic deformation processes.

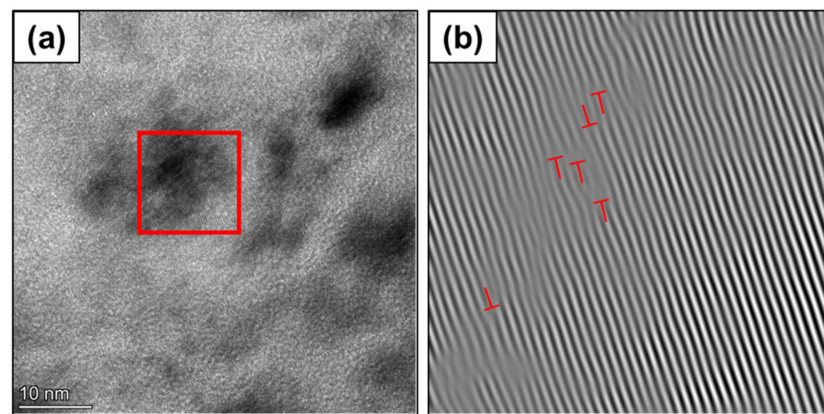


**Figure 6.** The interaction between the dislocations and the element segregation in the 945A-32h sample, (a) the high-resolution TEM image, (b) the inverse FFT of the red box in the Figure 6a.

#### 4.2. The Strengthening Mechanism of the Second Phase

After aging at 725 °C for 32 h, the 945A Ni-based superalloy exhibited a good strength improvement. The strength improvement was mainly from the precipitation hardening, as a large number of nanometer precipitates were observed in the microstructure. The effect of the nanometer precipitates during the plastic deformation process can be understood by the Orowan relationship [28]

$$\tau_{Orowan} = \left( \frac{Gb}{2\pi\sqrt{1-\nu}} \right) \left( \frac{1}{\lambda} \right) \log \left( \frac{D_p}{r_0} \right) \quad (1)$$

where  $\tau_{Orowan}$  is the Orowan stress (MPa),  $G$  is the shear modulus (MPa),  $b$  is the Burgers vector (m),  $\nu$  is the Poisson ratio,  $\lambda$  is the particle spacing (m),  $D_p$  is the mean planar diameter of the particle (m) and  $r_0$  is the dislocation core radius (m).

According to Equation (1), it can be seen that the distance between the particles and the size of the particles have a large impact on the improvement in the Orowan strengthening effect. The strengthening effect is inversely proportional to the spacing of the particles, and is proportional to the mean planar diameter of the particle. Aging treatment significantly changes the distance between the particles and the size of the particles. With the increase in the aging time, the proportion of nanometer precipitates increased, and the space between the particles decreased. After aging treatment, the size of the  $\gamma'$  phase particles was about 10–20 nm, and the distance between the  $\gamma'$  phase particles was about 5–10 nm, which is a small size and close spacing. Therefore, the strengthening effect of the Orowan mechanism

was increased. As the result, the compressive yield stress of the 945A Ni-based superalloy was significantly improved from 229 to 809 MPa.

## 5. Conclusions

In this study, the aging behavior of the wrought 945A Ni-based superalloy was investigated at 725 °C with different aging durations. The main conclusions are summarized as follows:

- (1) The compressive yield stress of the 945A Ni-based superalloy was significantly improved by the increase in aging time. Compressive yield stress increased from 229 to 809 MPa, an increase of more than 220%.
- (2) After aging at 725 °C for 32 h, a large proportion of precipitates occurred in the matrix. The precipitates contained  $\gamma'$  phase and carbide.
- (3) The formation of the  $\gamma'$  phase was stimulated by the residual dislocations.
- (4) The strengthening effect was attributed mainly to the large number of nanoscale precipitates of small size and close spacing after the aging treatment.

**Author Contributions:** Conceptualization, H.L. and J.S.; methodology, D.W.; software, D.W.; validation, H.L., D.W., L.Z., J.S. and W.W.; formal analysis, J.S.; investigation, H.L.; resources, H.L.; data curation, J.S.; writing—original draft preparation, H.L.; writing, review and editing, H.L., J.S. and L.Z.; visualization, H.L.; supervision, L.Z.; project administration, J.S.; funding acquisition, L.Z. All authors have read and agreed to the published version of the manuscript.

**Funding:** This work was funded by the Beibei Technology Innovation and Application Demonstration Project [2020-7], Major Science and Technology Project of Sinomach [SINOMAST-ZDZX-2018-05].

**Institutional Review Board Statement:** Not applicable.

**Informed Consent Statement:** Not applicable.

**Data Availability Statement:** All data generated or analyzed during this study are included in this article.

**Conflicts of Interest:** The authors declare no conflict of interest.

## References

1. Ayer, R.; Mueller, R.R.; Koo, J.Y.; Watkins, M. Acceptability criteria for alloy 718 for use in sour service. In Proceedings of the Thirteenth International Offshore and Polar Engineering Conference, Honolulu, HI, USA, 25–30 May 2003; pp. 75–82.
2. Ezugwu, E.O.; Wang, Z.M.; Machado, A.R. The machinability of nickel-based alloys: A review. *J. Mater. Process. Technol.* **1999**, *86*, 1–16. [[CrossRef](#)]
3. Ward, J. *The Last Defence against Corrosion: Alloy 945 and 945X*; Stainless Steel World: MECC Maastricht, The Netherlands, 2015; pp. 1–3.
4. Han, V.F.; Deb, P.; Chaturvedi, M.C. Coarsening behaviour of  $\gamma''$ - and  $\gamma'$ -particles in inconel alloy 718. *Met. Sci.* **1982**, *16*, 555–561. [[CrossRef](#)]
5. Hagel, W.C.; Beattie, H.J. Iron and Steel Institute Special Report. The Iron and Steel Institute: London, UK, 1964; Volume 98.
6. Hume-Rothery, W.; Mabbott, G.W.; Evans, K.M.C.; Carpenter, H.C.H. The freezing points, melting points, and solid solubility limits of the alloys of silver and copper with the elements of the b sub-groups. *Philosophical Transactions of the Royal Society of London. Ser. A Contain. Pap. Math. Phys. Character* **1934**, *233*, 1–97.
7. Rudman, P.; Stringer, J.; Jaffee, R.I. Hume-Rothery, Factors affecting the stability of metallic phases. In *Phase Stability in Metals and Alloys*; Rudman, P., Stringer, J., Jaffee, R.I., Eds.; McGraw-Hill: New York, NY, USA, 1967; pp. 3–23.
8. Chaturvedi, M.C.; Han, Y.-F. Strengthening mechanisms in Inconel 718 superalloy. *Met. Sci.* **1983**, *17*, 145–149. [[CrossRef](#)]
9. Oblak, J.M.; Paulonis, D.F.; Duvall, D.S. Coherency strengthening in Ni base alloys hardened by DO22  $\gamma'$  precipitates. *Metall. Trans.* **1974**, *5*, 143–153.
10. Yan, B.C.; Zhang, J.; Lou, L.H. Effect of boron additions on the microstructure and transverse properties of a directionally solidified superalloy. *Mater. Sci. Eng. A* **2008**, *474*, 39–47. [[CrossRef](#)]
11. Peng, P.; She, J.; Tang, A.; Zhang, J.; Zhou, S.; Xiong, X.; Pan, F. Novel continuous forging extrusion in a one-step extrusion process for bulk ultrafine magnesium alloy. *Mater. Sci. Eng. A* **2019**, *764*, 138144. [[CrossRef](#)]
12. She, J.; Peng, P.; Tang, A.T.; Zhang, J.Y.; Mao, J.J.; Liu, T.T.; Zhou, S.B.; Wang, Y.; Pan, F.S. Novel on-line twist extrusion process for bulk magnesium alloys. *Mater. Des.* **2019**, *182*, 108011. [[CrossRef](#)]

13. Peng, P.; Tang, A.; She, J.; Zhang, J.; Zhou, S.; Song, K.; Pan, F. Significant improvement in yield stress of Mg-Gd-Mn alloy by forming bimodal grain structure. *Mater. Sci. Eng. A* **2021**, *803*, 140569. [[CrossRef](#)]
14. She, J.; Zhou, S.B.; Peng, P.; Tang, A.T.; Wang, Y.; Pan, H.C.; Yang, C.L.; Pan, F.S. Improvement of strength-ductility balance by Mn addition in Mg-Ca extruded alloy. *Mater. Sci. Eng. A* **2020**, *772*. [[CrossRef](#)]
15. Ding, Q.; Li, S.; Chen, L.-Q.; Han, X.; Zhang, Z.; Yu, Q.; Li, J. Re segregation at interfacial dislocation network in a nickel-based superalloy. *Acta Mater.* **2018**, *154*, 137–146. [[CrossRef](#)]
16. Peng, P.; Zhang, K.; She, J.; Tang, A.; Zhang, J.; Song, K.; Yang, Q.; Pan, F. Role of second phases and grain boundaries on dynamic recrystallization behavior in ZK60 magnesium alloy. *J. Alloys Compd.* **2020**, *861*, 157958. [[CrossRef](#)]
17. Zhang, Y.; Jin, S.; Trimby, P.W.; Liao, X.; Murashkin, M.Y.; Valiev, R.Z.; Liu, J.; Cairney, J.M.; Ringer, S.P.; Sha, G. Dynamic precipitation, segregation and strengthening of an Al-Zn-Mg-Cu alloy (AA7075) processed by high-pressure torsion. *Acta Mater.* **2019**, *162*, 19–32. [[CrossRef](#)]
18. Huang, K.; Marthinsen, K.; Zhao, Q.; Logé, R.E. The double-edge effect of second-phase particles on the recrystallization behaviour and associated mechanical properties of metallic materials. *Prog. Mater. Sci.* **2018**, *92*, 284–359. [[CrossRef](#)]
19. Saleem, B.; Dong, H.B.; Patel, V. Effect of aging on the strength of corrosion-resistant incoloy alloys 945 and 945X: A microstructural perspective. *Mater. Sci. Eng. A* **2019**, *748*, 327–336. [[CrossRef](#)]
20. Devaux, A.; Nazé, L.; Molins, R.; Pineau, A.; Organista, A.; Guédou, J.Y.; Uginet, J.F.; Héritier, P. Gamma double prime precipitation kinetic in Alloy 718. *Mater. Sci. Eng. A* **2008**, *486*, 117–122. [[CrossRef](#)]
21. Dong, C.; Liu, Z.; Wang, X.; Liu, Z.; Chen, Z.; Bao, H. Formation behavior of long needle-like M23C6 carbides in a nickel-based alloy without  $\gamma'$  phase during long time aging. *J. Alloys Compd.* **2020**, *821*, 153529. [[CrossRef](#)]
22. Valle, L.C.M.; Santana, A.I.C.; Rezende, M.C.; Dille, J.; Mattos, O.R.; de Almeida, L.H. The influence of heat treatments on the corrosion behaviour of nickel-based alloy 718. *J. Alloys Compd.* **2019**, *809*, 151781. [[CrossRef](#)]
23. Whitmore, L.; Leitner, H.; Povoden-Karadeniz, E.; Radis, R.; Stockinger, M. Transmission electron microscopy of single and double aged 718Plus superalloy. *Mater. Sci. Eng. A* **2012**, *534*, 413–423. [[CrossRef](#)]
24. Liu, Y.; Guo, Q.; Li, C.; Mei, Y.; Zhou, X.; Huang, Y.; Li, H. Recent progress on evolution of precipitates in inconel 718 superalloy. *Acta Metall. Sin.* **2016**, *52*, 1259–1266.
25. Mannan, S. Time-Temperature-Transformation Diagram of Alloy 945. 7th International Symposium on Superalloy 718 and Derivatives, Pittsburgh, PA, USA, 10–13 October 2010; Ott, E.A., Groh, J.R., Banik, A., Dempster, I., Eds.; TMS: Pittsburgh, PA, USA, 2010.
26. Bobylev, S.V.; Enikeev, N.A.; Sheinerman, A.G.; Valiev, R.Z. Strength enhancement induced by grain boundary solute segregations in ultrafine-grained alloys. *Int. J. Plast.* **2019**, *123*, 133–144. [[CrossRef](#)]
27. Nie, J.F.; Zhu, Y.M.; Liu, J.Z.; Fang, X.Y. Periodic Segregation of Solute Atoms in Fully Coherent Twin Boundaries. *Science* **2013**, *340*, 957. [[CrossRef](#)] [[PubMed](#)]
28. Embury, J.D.; Lloyd, D.J.; Ramachandran, T.R. 22—Strengthening mechanisms in aluminum alloys. In *Treatise on Materials Science & Technology*; Vasudevan, A.K., Doherty, R.D., Eds.; Elsevier: Amsterdam, The Netherlands, 1989; pp. 579–601.